Temperature-Dependent Crystalline–Amorphous Structures in Linear Polyethylene: Surface Melting and the Thickness of the Amorphous Layers

T. Albrecht* and G. Strobl

Fakultät für Physik, Universität Freiburg, Hermann-Herder-Strasse 3, D-79104 Freiburg, Germany

Received March 14, 1995; Revised Manuscript Received May 31, 1995[⊗]

ABSTRACT: SAXS experiments on isothermally crystallized polyethylene reveal a clear temperature dependence of the crystalline–amorphous structure over a broad range of temperatures below the crystallization temperature. This phenomenon is analyzed using SAXS in combination with dilatometry, which allows for a quantitative determination of structure parameters. Reversible surface melting is shown to be the process responsible for the phenomenon. The thickness of the amorphous layers reflects a local equilibrium within the kinetically controlled amorphous–crystalline superstructure. Existing models which try to explain this behavior are reviewed and compared to the experimental results. After a slight modification is introduced to the theoretical considerations, the data can be adequately represented by a model which describes the amorphous layers as an entanglement network. To the deformations caused by surface melting the network responds with forces opposing further crystallization, thus leading to a temperature-dependent equilibrium.

Introduction

Structure formation by crystallization in polyethylene is a complex process and has been an object of research for a long time. There are three main contributing processes: crystal growth, isothermal thickening, and "partial melting", the last term being used for temperature-dependent continuous changes in the crystallinity. This work is concerned with the analysis of the third process. Polyethylene crystallizes in the form of thin lamellar crystals whose thickness depends on the temperature T_c at which the crystallization takes place. After completion of the crystallization at T_c, subsequent cooling of the sample results in a further rise of the crystallinity. On heating the sample, the reverse process occurs, setting in already far below the temperature of final melting. In the discussion of the physical processes underlying this phenomenon, two different mechanisms are considered. First, partial crystallization can be connected with the formation of new crystalline lamellae. Second, a reversible thickening of the existing lamellae can be envisaged. Although several authors have addressed this question,[4,10,13] a distinction is difficult and has so far not been unambiguous. Tanabe et al.[13] published the most detailed investigation of the temperature-dependent structure changes by means of small-angle X-ray scattering. But in this case a complete quantitative analysis of his data was difficult because of the presence of parasitic scattering intensity at very small angles. Although hints for a reversible thickening of the lamellae were observed, this process could not be identified unambiguously as the dominant contribution responsible for the structural changes.

In this work we also apply small-angle X-ray scattering, a technique which is particularly suited for in situ observations of the structure at different temperatures, in combination with dilatometry. This allows for a quantitative determination of the specific inner surface and thus a distinction between the two mechanisms. As will be shown, the results can also be derived from small-angle X-ray scattering alone by a detailed analysis of the structure factor.

[⊗] Abstract published in *Advance ACS Abstracts,* July 15, 1995.

Theory of Small-Angle X-ray Scattering: Method of Data Analysis

Structural Parameters and the Interface Distribution Function. The crystalline–amorphous structure of partially crystalline polymers is usually analyzed in terms of a one-dimensional stack model, the stacks consisting of crystalline lamellae separated by amorphous layers. The lamellae are assumed to be much extended laterally, so that the lateral boundaries have no effect on the scattering.

The methods to determine the structure parameters of the stack, i.e., the thicknesses d_a and d_c of the amorphous and the crystalline layers, respectively, are well established.[9,12] The scattering intensity $I(s)$ can be related to the one-dimensional electron density correlation function $K(z)$, which is defined as the average

$$K(z) = \langle \delta\varrho(z')\delta\varrho(z'+z)\rangle_{z'} \tag{1}$$

whereby $\delta\varrho$ denotes the deviation of the density from the mean value

$$\delta\varrho(z) = \varrho(z) - \langle\varrho\rangle \tag{2}$$

From the scattering intensity $I(s)$ the correlation function $K(z)$ can be determined by the cosine transformation

$$K(z) = 2\int_0^\infty 2\pi s^2 I(s)\cos(2\pi sz)\,\mathrm{d}s \qquad \text{with } s = \frac{2}{\lambda}\sin\frac{\theta}{2} \tag{3}$$

Ruland applied the concept of the interface distribution for the determination of the structure parameters.[9] The interface distribution function is directly related to the second derivative of the correlation function $K''(z)$, as the latter can be expressed as follows:

$$K''(z) = \frac{O_s}{2}\Delta\varrho^2[h_a(z) + h_c(z) - 2h_{ac}(z) + h_{aca}(z) + h_{acc}(z) + \ldots] \tag{4}$$

Here O_s denotes the specific inner surface, and $\Delta\varrho$ gives the electron density difference between the crystalline and amorphous regions. The expression between the brackets is set up of various distribution functions, all of them associated with distances between interfaces.

0024-9297/95/2228-5827$09.00/0

The subscripts denote which amorphous and crystalline phases are traversed while going from one interface to the other. Of practical importance are only the first three contributions h_a, h_c, and h_{ac}. They give the distributions of the thicknesses of the amorphous and the crystalline layers and of the sum of both, which determines the long period L. An example based on simulated data is shown in Figure 1.

As proved by Ruland, $K''(z)$ can be directly calculated from the scattering intensity $I(s)$:

$$K''(z) = 16\pi^3 \int_0^\infty ds\, [\lim_{s\to\infty} I(s)s^4 - I(s)s^4] \cos(2\pi sz) \quad (5)$$

Before applying eq 5, the background intensity due to the density fluctuations within the individual phases has to be subtracted. The calculation of the interface distribution function by the Fourier transform of eq 5 usually requires a smoothing of the data in order to reduce the effect of noise. Furthermore, the truncation effect following from the finite measuring range has to be avoided. This can be achieved by a multiplication with a Gaussian function of appropriate width before calculating the cosine transform.

The crystallinity (by volume) ω_c and the specific inner surface O_s can be derived from particular properties of $K(z)$ in the vicinity of $r = 0$. The following equations hold:

$$4\pi \int_0^\infty ds\, s^2 I(s) = K(0) = \omega_c(1 - \omega_c)\Delta\varrho^2 \quad (6)$$

$$\lim_{s\to\infty} I(s)s^4 = -\frac{K'(0)}{4\pi^3} = \frac{O_s \Delta\varrho^2}{8\pi^3} := P \quad (7)$$

Equation 7 is called Porod's law. As can be seen in eq 5, it is exactly this constant which has to be subtracted if $K''(z)$ and thus the interface distribution function is to be calculated.

For the question addressed in this work, a further parameter, $K''(0)$, is very useful. In a recent publication we showed that $K''(0)$ is connected to the specific length of "edges" in the sample.[1] These edges are the boundary lines of the inner surfaces and are found either on free lateral faces of crystallites or along the lines of encounter of two crystallites. Figure 2 provides a sketch for illustration. The relation between $K''(0)$ and the edge concentration is

$$K''(0) = 16\pi^3 \int_0^\infty ds\, [\lim_{s\to\infty} I(s)s^4 - I(s)s^4] = \frac{1}{\pi}\langle L_s w(\alpha)\rangle v \Delta\varrho^2 \quad (8)$$

whereby L_s designates the length of edges per unit volume and $w(\alpha)$ is a weighting factor dependent on the angle α enclosed by the crossing interfaces

$$w(\alpha) = 1 + (\pi - \alpha)\cot(\alpha) \quad (9)$$

Formally, $K''(0)$ is related to the amount of neighboring interfaces with zero distance. Therefore, in case of a one-dimensional stack of laterally extended lamellae, $K''(0)$ should be equal to, or at least close to, zero. The assumption that data can be described by a one-dimensional stack model implies that any contribution to the scattering intensity from lateral surfaces and the edges can be neglected. Indeed, the condition $K''(0) = 0$ can be used in order to check whether the evaluation procedure based on the one-dimensional model is consistent with the scattering curve. In reverse, being sure about the one-dimensionality of a system, the requirement $K''(0) = 0$ may aid in determining the Porod constant P. Extracting it from the asymptotic tail of the scattering intensity $I(s)$ alone in the presence of a much larger background is sometimes difficult.

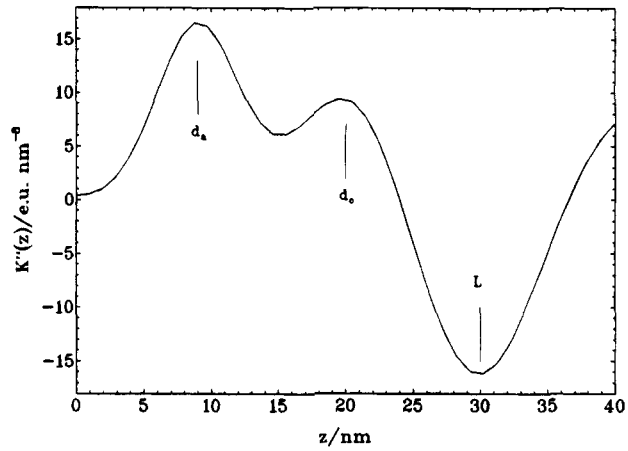

Figure 1. $K''(z)$ as calculated for a simulated data set with $d_a = 9$ nm and $d_c = 21$ nm.

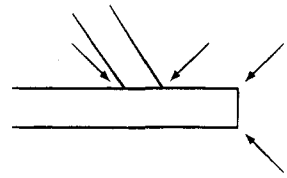

Figure 2. Illustration of the concept of edges at the boundaries and lines of encounter of inner surfaces.

Deviations from the one-dimensional structure, as they could result, for example, from the generation of new small crystallites during cooling, would show up in a rising value of $K''(0)$.

Experiments

SAXS experiments were carried out with a conventional X-ray tube and a Kratky compact camera equipped with a temperature-controlled sample holder. Measurements were conducted with two different detector systems, either a position-sensitive metal wire counter or a scintillation counter mounted on a PC-controlled stepper system. As the camera is equipped with a slit focus, the data had to be deconvoluted. This was achieved by applying the desmearing algorithm by Strobl.[11] Using the moving-slit method for measurements of the primary beam intensity, absolute intensities were obtained.

Samples. In this work partial melting in two polyethylene samples with different molecular weight was investigated. The first sample was a commercially available linear polyethylene (BASF Lupolen 6011L). From the work of Kanig by electron microscopy, the lamellar nature of the crystallites in this material is well established.[5] Secondly, we studied a linear polyethylene with low molecular weight of $M_w \approx 17000$. As indicated again by electron microscopy,[7] samples of low molecular weight generally form more perfect lamellar structures, and this was indeed confirmed by the obtained SAXS curves. The material was synthesized with a metallocene catalyst.[2] The molecular weight was determined by viscosity measurements. Samples were molten under vacuum and subsequently isothermally crystallized in the SAXS camera. After completion of the primary crystallization, samples exhibit during cooling and reheating temperature-dependent reversible changes in the structure, as reflected in the scattering intensity.

Dilatometry. The SAXS experiments were complemented by a measurement of the density of the samples. First, the density at 25 °C was determined by buoyancy measurements.

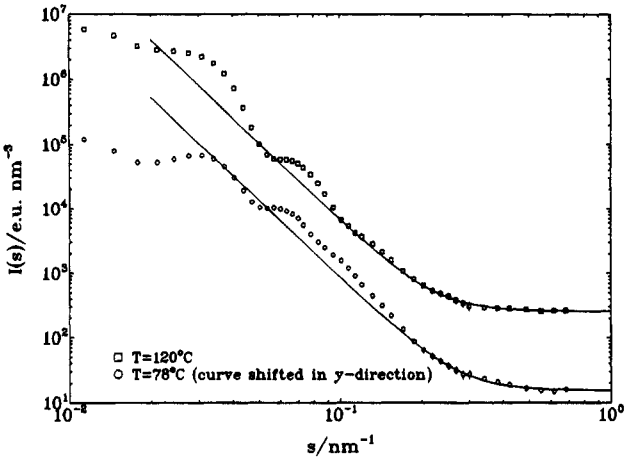

Figure 3. Sample of polyethylene, $M_w \approx 17000$: SAXS intensity $I(s)$ for $T = 120$ and 78 °C. The continuous lines give the sum of the Porod scattering and a background due to density fluctuations.

Then the effects of partial melting were monitored using a mercury-filled dilatometer. The measurements were carried out up to temperatures of about 170 °C, heating the dilatometer in an oil bath. Assuming that the amorphous parts in the partially crystalline material have the same density as it follows by an extrapolation from the melt, the quantity $\omega_c\Delta\varrho$ can be obtained by subtracting this amorphous density, ϱ_a, from the density ϱ, as determined for the partially crystalline material.

$$\varrho = \varrho_a + \omega_c(\varrho_c - \varrho_a) \tag{10}$$

$$\varrho - \varrho_a = \omega_c\Delta\varrho \tag{11}$$

Results

We begin with the results obtained for the low molecular weight polyethylene. Figure 3 shows two SAXS curves measured at different temperatures during cooling, subsequent to an isothermal crystallization at $T_c = 120$ °C. The double-logarithmic representation reveals that the data agree for high values of s with Porod's law. The continuous lines give the sum of the Porod contribution and a background due to density fluctuations within the single phases. The curve obtained at 78 °C shows deviations from the Porod limit up to higher values of s, indicating interferences due to smaller structures. The condition $K''(0) = 0$ is fulfilled in both cases. Hence, effects of edges, if they exist at all, are negligible. Note the absence of any indication for a transition zone between the crystalline and amorphous phases, since this would result in a decay even stronger than Porod's law $I \sim s^{-4}$. At both temperatures maxima in the scattering intensity at $s \approx 0.032$ nm^{-1} and $s \approx 0.064$ nm^{-1} can be seen, corresponding to a long period of about 30 nm. Apart from this common feature, the structure factors are quite different. In particular, the curve for $T = 78$ °C has another broad maximum centered around $s \approx 0.11$ nm^{-1}.

The changes in the structure factor can be understood when observing the corresponding changes in the interface distribution function, as shown in Figure 4. As in the numerical example in Figure 1, three contributions, due to the amorphous and the crystalline layers and—with opposite sign—the long period, can be seen. Changing from 120 to 78 °C, the first contribution, attributed to the thicknesses of the amorphous layers, is shifted to the left, while the contribution associated

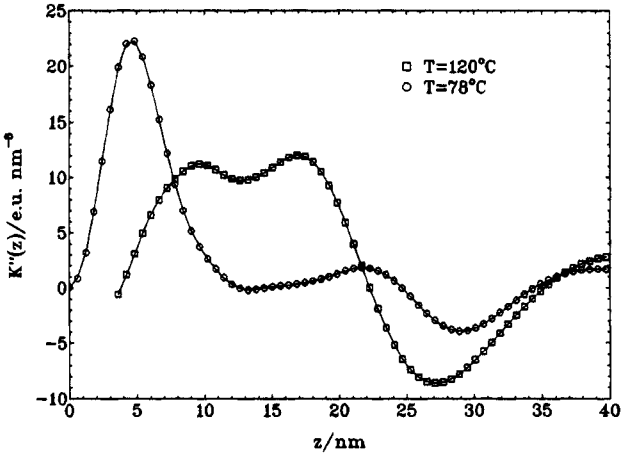

Figure 4. Sample of polyethylene, $M_w \approx 17000$: function $K''(z)$ for $T = 120$ und 78 °C, as calculated from the data represented in Figure 3.

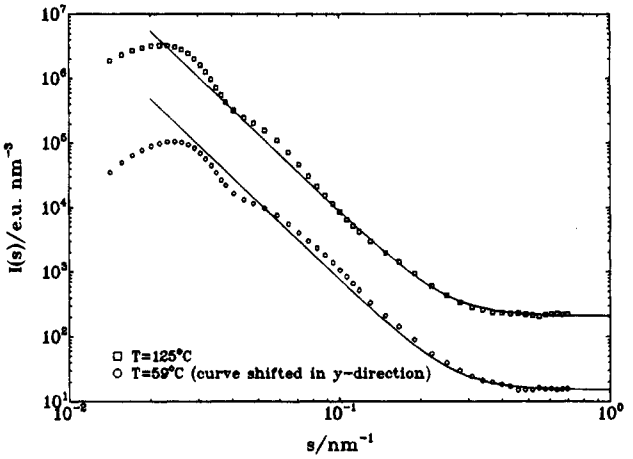

Figure 5. Sample of PE (Lupolen 6011 L): SAXS intensity $I(s)$ for $T = 125$ and 59 °C. The continuous lines give the sum of the Porod scattering and a background due to density fluctuations.

with the crystalline layers is shifted toward higher values. The latter shift leads to an overlap with the negative contribution due to the long period and thus to an apparent decrease of the amplitude of this crystalline component. As a consequence, the still isolated contribution of the amorphous layers with its center at $d_a = 4.5$ nm becomes dominant and results in the maximum at $s = 1/2d_a \approx 0.11$ nm^{-1}. Hence, we have clear evidence for a decrease of the thickness of the amorphous layers, being accompanied by a simultaneous increase of the crystallite thicknesses. The observations are indicative for a process of surface crystallization, or during heating, a surface melting.

Further confirmation comes from an analysis of the scattering data in combination with dilatometry, allowing for a determination of the crystallinity and the specific inner surface. For this second experiment the other material—Lupolen 6011—was chosen. The sample was isothermally crystallized at $T_c = 124$ °C. Figures 5 and 6 show that the scattering intensity and the interface distribution function exhibit the same temperature-dependent changes as for the first sample. The distribution of the crystallite thickness seems to broader than in the sample with lower molecular weight. The resulting values for the thickness of the amorphous layers d_a—derived from the maxima in the interface distribution functions—are shown as a function of temperature in Figure 7. Both the values obtained during

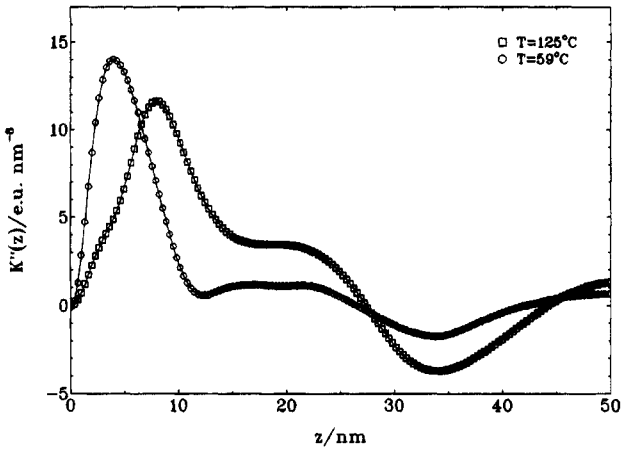

Figure 6. Sample of PE (Lupolen 6011 L): function $K''(z)$ for T = 125 and 59 °C, as calculated from the data represented in Figure 5.

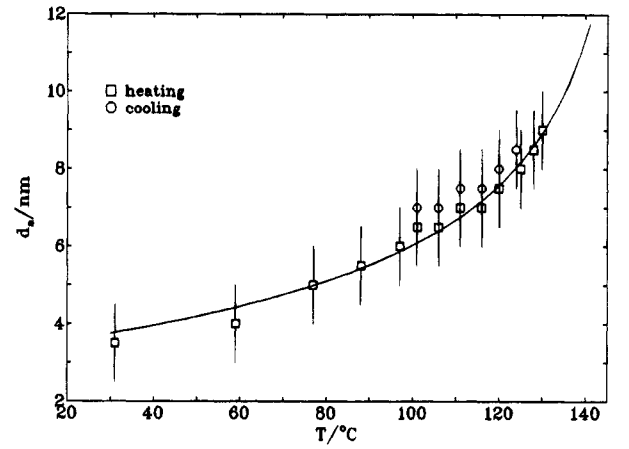

Figure 7. Sample of PE (Lupolen 6011 L): Thickness d_a of the amorphous layers as a function of temperature, derived from the characteristic maximum in the function $K''(z)$. The continuous line shows a fit based on eq 37. Data obtained during a heating and during a cooling cycle are shown for comparison.

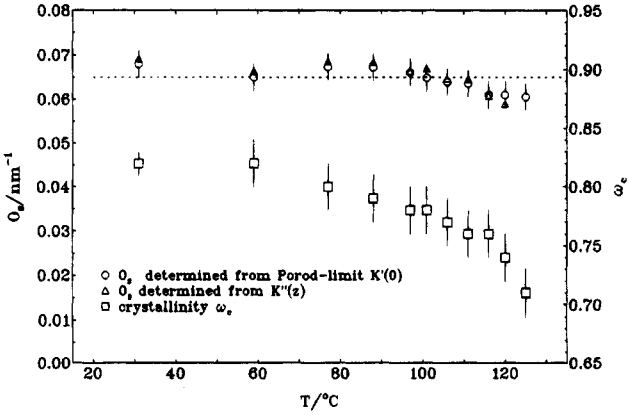

Figure 8. Sample of PE (Lupolen 6011 L): crystallinity ω_c and specific inner surface O_s as a function of temperature as observed during heating. ω_c is derived from the invariant $K(0)$ and dilatometric measurements. The two values for O_s are based on $K'(0)$ and $K''(z)$, respectively.

heating and cooling are included, and comparison demonstrates that the changes are perfectly reversible.

In Figure 8 the results of the data evaluation are presented. As expected, there is a pronounced temperature dependence of the crystallinity ω_c. The crucial quantity—the specific inner surface O_s—remains constant within 10% over the whole temperature range. The two values shown for O_s in Figure 8 result from two methods of data evaluation, thus providing a check of consistency. O_s can be determined either from the asymptotic behavior of the scattering intensity using Porod's law or from an integration over the first contribution $(O_s/2)\Delta\varrho^2 h_a(z)$ of the interface distribution function, regarding that $\int_0^\infty h_a(z)\,dz = 1$. Both methods give the same results, thus confirming that the decrease of the amorphous layer thickness is not produced by the generation of new crystallites but by a thickening of the existing lamellae.

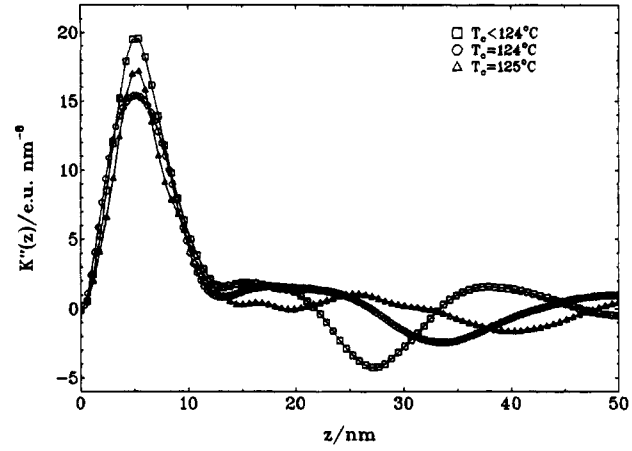

Figure 9. Sample of PE (Lupolen 6011 L): function $K''(z)$ for T = 88 °C obtained for samples crystallized at different temperatures. Structures have different long periods but identical amorphous layer thicknesses.

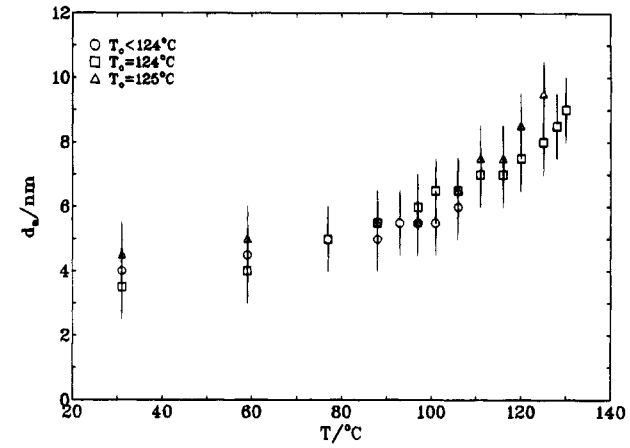

Figure 10. Sample of PE (Lupolen 6011 L): thickness d_a of the amorphous layers as a function of temperature, determined from the characteristic maxima in the function $K''(z)$. The samples were crystallized at the indicated temperatures.

The temperature dependence of the thickness d_a being established, we proceed to the question of whether d_a is affected by the conditions of primary crystallization, as it is the case for d_c. Experiments on samples which have been crystallized at different temperatures show that, indeed, d_a depends only on the actual temperature and is independent of the thermal history. Figure 9 demonstrates this fact. The interface distribution functions of three samples, crystallized at different T_c's and subsequently cooled to 88 °C, show clearly different long periods and different thicknesses of the crystalline layer, whereas the contributions of the amorphous layers are practically identical. Figure 10 shows that this behavior pertains over the full temperature range.

Conclusions and Theoretical Models

Analysis of the experiment, including both the combined evaluation of SAXS data and dilatometry and the discussion of the structure factor by means of the interface distribution function, confirms that surface melting is the dominant process responsible for partial melting and crystallization in linear polyethylene.

Furthermore, it could be shown that the thickness of the amorphous layers depends only on temperature and not on the thermal history, in clear contrast to the thickness of the crystalline lamellae. It appears that d_a is determined by, and thus reflects, an equilibrium of local nature which exists within the kinetically controlled crystalline–amorphous superstructure.

A necessary prerequisite for the observed surface crystallization and melting processes is a high mobility of the chains in the crystals in PE. It is provided by the α-relaxation, which allows for an exchange between the two phases. Since a longitudinal chain transport is not found in all polymers, surface crystallization and melting is not a general phenomenon. For example, recently we studied partial melting processes in polypropylene.[1] This material does not exhibit a crystalline relaxation process similar to the α-process in PE, and, indeed, surface melting does not occur.

Fischer,[3] Zachmann,[14] Mansfield,[6] and Rieger[8] developed models for a description of surface melting. We first revisit these approaches and test them against the experimental data we obtained. Subsequently, we suggest some modifications in order to remove existing deficiencies.

All models start with the assumption that the possible conformations of the chains in the amorphous layers are restricted compared to a free chain. In the treatments of Fischer and Zachmann, the amorphous layers are considered to be made up of loops which emanate from the crystallites at fixed points. An entropic force arises from the shortening of a loop as it follows from a thickening of the crystallites, thus opposing the tendency toward crystallization. Mansfield and Rieger focus in their treatment on the effect of the entanglements trapped in the amorphous regions.

In Fischer and Zachmann's model, first the partition function for a Gaussian chain (N segments with length b) with ends fixed at a distance R is formulated:

$$W(R^2,N) = Z^N\left(\frac{2\pi N b^2}{3}\right)^{-3/2} \exp\left(-\frac{3R^2}{2Nb^2}\right) \quad (12)$$

Z^N is the partition function of the same chain without constraints. If the amorphous phase is made up of ν chains, the free energy G_a amounts to

$$G_a = -\frac{\nu}{\beta}\ln W = \frac{\nu}{\beta}\left[N\beta\mu_a + \frac{3}{2}\ln\left(\frac{2\pi b^2}{3}\right) + \frac{3}{2}\ln N + \frac{3R^2}{2Nb^2}\right] \quad (13)$$

with

$$\beta\mu_a = -\ln Z \left(\beta := \frac{1}{k_B T}\right)$$

μ_a being the chemical potential per segment of the amorphous phase. Next the two crystallites adjacent to the amorphous layer are included in the consideration. As the interfaces are only shifted, we must not account for the excess free energy associated with them and may represent the total free energy G as the sum of the contributions from the crystalline and the amorphous parts. Let N_c be the number of segments in the crystalline phase, μ_c the chemical potential per segment in the crystals, and $N_a = \nu N$ the number of segments in the amorphous phase. It then follows

$$\beta G = N_c\beta\mu_c + \nu\frac{3}{2}\ln\left(\frac{2\pi b^2}{3}\right) + \nu N\beta\mu_a + \nu\frac{3}{2}\ln N + \nu\frac{3R^2}{2Nb^2} \quad (14)$$

N_a adjusts so that a state of minimal free energy is reached under the condition $N_a + N_c = \text{const}$. Minimization results in the following equation for the loop length N:

$$\beta(\mu_a - \mu_c) = \beta\Delta\mu = \frac{3R^2}{2N^2b^2} - \frac{3}{2N} \quad (15)$$

The right-hand side represents an extra contribution to the chemical potential of the amorphous chains. Equation 15 is solved by

$$\frac{1}{N} = \frac{b^2}{R^2}\left(\frac{1}{2} + \left(\frac{1}{4} + \frac{2R^2}{3b^2}\beta\Delta\mu\right)^{1/2}\right) \quad (16)$$

At the melting temperature, for $\Delta\mu = 0$, N assumes the value

$$\frac{1}{N_0} = \frac{b^2}{R^2} \quad (17)$$

which corresponds to the mean value of a free chain. Assuming the thickness d_a of the amorphous layers to be proportional to the length N of the individual chains,

$$N = \gamma d_a \quad (18)$$

one arrives at an equation for d_a

$$\frac{1}{d_a} = \frac{1}{d_0}\left(\frac{1}{2} + \left(\frac{1}{4} + \frac{2}{3}\gamma d_0\beta\Delta\mu\right)^{1/2}\right) \quad (19)$$

Here d_0 denotes the thickness of the amorphous layers for $\Delta\mu = 0$.

Near the melting point the following approximation holds for $\Delta\mu$:[6]

$$\Delta\mu \approx \frac{\Delta H_m}{T_f}(T_f - T) \quad (20)$$

ΔH_m is the enthalpy of fusion per segment, and T_f is the equilibrium melting temperature. In order to assign numeric values to the parameters, it is necessary to specify the length of the unit segment used in the calculations above. For the chain to be Gaussian, one has of course to use the Kuhn segment. But as in the final equation 19 only the product $\gamma d_0\Delta\mu = N_0\Delta\mu$ appears, which is independent of the length of the unit segment, in the following the unit segment is chosen to be the chemical repeat unit CH_2. For polyethylene we have

$$\Delta H_m = 4\ \text{kJ/mol}, \qquad T_f = 414\ \text{K} \quad (21)$$

and therefore

$$\beta\Delta\mu = \frac{\Delta H_m T_f - T}{k_B T_f \quad T} = 1.17\frac{T_f - T}{T} \tag{22}$$

As it turns out, the experimental data obtained from the sample of Lupolen with $T_c = 124$ °C can indeed be fitted by eq 19, resulting in the following values for the parameters d_0 and γ:

$$d_0 = 12.6 \text{ nm}, \qquad \gamma = 2.1 \text{ nm}^{-1} \tag{23}$$

However, considering this result, a simple check shows that the resulting value for γ is unreasonable. γ is related to the segment density, ϱ_s, and the number n_l of loops per unit area of the crystallite surface. Since two crystallites contribute to one amorphous layer, we have

$$\frac{2n_l N}{\varrho_s} = d_a \tag{24}$$

and therefore

$$\gamma = \frac{\varrho_s}{2n_l} \tag{25}$$

As an estimate, n_l is about 1/2·1/2 of the number n_c of chains per unit area in the crystalline lamellae. The second factor 1/2 follows from the fact that the chains in the amorphous layers are isotropically oriented, leading to a reduction of the flux of chains per unit area compared to the uniaxially oriented chains in the crystallites. Fifty percent of the emanating chains cannot penetrate further into the amorphous regions and have to fold back. Neglecting the density difference between the amorphous and the crystalline regions, n_c is related to the segment density ϱ_s and the distance c between two carbon atoms of a chain in the crystal.

$$n_c = \varrho_s c \tag{26}$$

Then γ follows as

$$\gamma = \frac{2}{c} = \frac{2}{0.127 \text{ nm}} = 15.7 \text{ nm}^{-1} \tag{27}$$

Comparison with the value derived from the experiment shows a large discrepancy, indicating that with the assumptions made above, the observations cannot be explained.

Mansfield and Rieger's approach focuses on effects of the trapped entanglements rather than employing the loop picture. The amorphous layers contain a fixed number of entanglements, thus building up a permanent network. The treatment considers the deformation of this network resulting from surface melting. The entanglements are treated as slip-links, the subchains between two entanglements as Gaussian chains. Formally, the treatment leads to similar expressions as for the loop model, the difference being that now the subchains between entanglements constitute the basic units of the system. For the treatment an equation describing the deformation of the network is needed. $\langle R^2\rangle$ is now the squared distance between two slip-links, which in the isotropic state is the sum of three equal components:

$$\langle R^2\rangle = \langle R_{x0}{}^2\rangle + \langle R_{y0}{}^2\rangle + \langle R_{z0}{}^2\rangle = N_0 b^2 \tag{28}$$

Mansfield assumes that only the z-component of $\langle R^2\rangle$ is affected by a change in the thickness d_a of the amorphous layers. As in classical rubber elasticity theory, an affine transformation between d_a and $\langle R_z{}^2\rangle^{1/2}$ is assumed, resulting in the following equation for $R_z{}^2$:

$$\langle R_z{}^2\rangle = \frac{1}{3}N_0 b^2\left(\frac{d_a}{d_0}\right)^2 = \frac{1}{3}N_0 b^2\left(\frac{N}{N_0}\right)^2 \tag{29}$$

Inserting the resulting expression for $\langle R^2\rangle$ in eq 14, minimization of the free energy gives the following expression for N:

$$\beta\Delta\mu = \frac{N_0}{N^2} - \frac{3}{2N} - \frac{1}{2N_0} \tag{30}$$

This equation, as derived by Mansfield and Rieger, has a deficiency concerning the solution for $\Delta\mu = 0$. It is given by

$$\frac{1}{N}(\Delta\mu = 0) = \frac{1}{N_0}\left(\frac{3}{4} + \left(\frac{17}{16}\right)^{1/2}\right) \tag{31}$$

Hence, the treatment predicts that even at the melting temperature, the chains are in an anisotropic state, although no more forces are acting, and this looks unreasonable.

At this point we suggest a modification of the model. We assume that the treatment of all the subchains as independent Gaussian chains is an approximation which is too crude. On the same level of approximation as in the first model, one would have to treat the whole chain, whose ends are fixed in the crystal and which consists of say m subchains, as the independent unit. If we now take into account that there are several possibilities to subdivide a chain of length mN into m subchains, an additional entropical contribution in the free energy of the amorphous layers shows up. In a first approximation this contribution can be estimated by simply counting the number k of possibilities to distribute the fixed number of slip-links m along the chain of length mN. The resulting expression for the free energy G of the system is analogous to eq 14:

$$\beta G = N_0\beta\mu_c + \nu m\left[\frac{3}{2}\ln\left(\frac{2\pi b^2}{3}\right) + N\beta\mu_a + \frac{3}{2}\ln N + \frac{3R^2}{2Nb^2}\right] - \nu \ln k \tag{32}$$

Only the leading N-dependent term of the additional entropical contribution has to be considered for the minimization of G:

$$\ln k = \ln\left(\frac{Nm}{m}\right) = \ln(Nm)! - \ln(Nm - m)! - \ln m! \approx Nm\ln Nm - Nm - (N-1)m\ln((N-1)m) + (N-1)m + f(m) \approx m\ln Nm + g(m) = m\ln N + h(m) \tag{33}$$

Minimization of the free energy G with respect to N_a leads now to the following equation for N:

$$\beta\Delta\mu = \frac{N_0}{N^2} - \frac{1}{2N} - \frac{1}{2N_0} \tag{34}$$

with the solution

$$\frac{1}{N} = \frac{1}{N_0}\left(\frac{1}{4} + \left(\frac{9}{16} + N_0\beta\Delta\mu\right)^{1/2}\right) \tag{35}$$

This modification already gives the correct behavior for $\Delta\mu = 0$.

$$\frac{1}{N} = \frac{1}{N_0} \tag{36}$$

Using eq 18, we get again an expression for the thickness of the amorphous layers:

$$\frac{1}{d_a} = \frac{1}{d_0}\left(\frac{1}{4} + \left(\frac{9}{16} + N_0\beta\Delta\mu\right)^{1/2}\right) \tag{37}$$

Recall that $\Delta\mu$ is given by eq 20.

Equation 37 provides a satisfactory representation of the experimental data, as shown in Figure 7. The fit was obtained using the parameters

$$d_0 = 11.8 \text{ nm} \qquad N_0 = 18 \tag{38}$$

The corresponding number n_s of subchains participating in surface melting per unit area of adjacent crystallites can be calculated in analogy to eq 24:

$$n_s = \frac{\varrho_s d_0}{2N_0} \approx 14 \text{ nm}^{-2} \qquad \text{whereby } \varrho_s \approx 43 \text{ nm}^{-3} \tag{39}$$

On the other hand, the number of loops or tie molecules per unit area of the crystallites was

$$n_l = \frac{n_c}{4} = \frac{\varrho_s c}{4} \approx 1.4 \text{ nm}^{-2} \tag{40}$$

Comparison of n_s and n_l indicates that each loop (or tie molecule) is divided into 10 subchains between entanglements.

In conclusion, a model which describes the chain parts in the amorphous regions as loops or tie molecules, which are subdivided by mobile slip-links into several subchains, provides a satisfactory representation of the experimental data. Partial melting is driven by the increase in the entropy of the subchains, resulting from an increase in their average length.

Acknowledgment. We thank B. Heck for assistance in the SAXS measurements. Support of this work by the Deutsche Forschungsgemeinschaft (SFB 60, Freiburg) is gratefully acknowledged.

References and Notes

(1) Albrecht, T.; Strobl, G. R., to be published.
(2) Chien, J. W. C. *J. Polym. Sci., Polym. Chem.* **1990**, *28*, 15.
(3) Fischer, E. W. *Kolloid Z. Z. Polym.* **1967**, *218*, 97.
(4) Fischer, E. W. *Kolloid Z. Z. Polym.* **1969**, *231*, 458.
(5) Kanig, G. *Colloid Polym. Sci.* **1982**, *260*, 356.
(6) Mansfield, M. L. *Macromolecules* **1987**, *20*, 1384.
(7) Michler, G. H. *Kunststoff-Mikromechanik*; Hanser: München, Wien, 1992.
(8) Rieger, J.; Mansfield, M. L. *Macromolecules* **1989**, *22*, 3810.
(9) Ruland, W. *Colloid Polym. Sci.* **1977**. *255*, 417.
(10) Schultz, J. M.; Fischer, E. W.; Schaumburg, O.; Zachmann, H. G. *J. Polym. Sci., Polym. Phys. Ed.* **1980**, *18*, 239.
(11) Strobl, G. R. *Acta Crystallogr.* **1970**, *A26*, 367.
(12) Strobl, G. R.; Schneider, M. *J. Polym. Sci.* **1980**, *18*, 1343.
(13) Tanabe, Y.; Strobl, G. R.; Fischer, E. W. *Polymer* **1986**, *27*, 1147.
(14) Zachmann, H. G. *Kolloid Z. Z. Polym.* **1969**, *231*, 504.

MA950329I